




TECHNICAL ARTICLE

Experimental Investigation on Carbon Diffusion at the Solid–Liquid Interface During Scrap Melting in the Steelmaking Process

MING GAO,¹ JIN TAO GAO,¹ YAN LING ZHANG ^{1,2}
and SHU FENG YANG¹

1.—State Key Laboratory of Advanced Metallurgy, University of Science and Technology Beijing, Beijing 100083, China. 2.—e-mail: zhangyanling@metall.ustb.edu.cn

Carbon diffusion at the solid–liquid interface is of fundamental importance in scrap melting. Herein, the scrap microstructure at the melt interface and the carbon and silicon distributions are described using optical microscopy and electron microprobe analysis (EPMA). The microstructural path from the surface to the interior of the scrap was primary carbide → acicular martensite → dislocation martensite (original structure). The corresponding carbon concentration gradient was $> 4 \text{ wt.}\%$ → $1\text{--}1.5 \text{ wt.}\%$ → $0.2 \text{ wt.}\%$. This was consistent with the observed microstructural changes. Furthermore, the depth of the carbon diffusion layer was $200 \mu\text{m}$ and $220 \mu\text{m}$ at 1300°C and 1350°C , respectively. The silicon-enriched layer may be a retarding factor for carbon dissolution. The area of the austenite phase region in the Fe-Fe₃C phase diagram was reduced owing to the presence of silicon. Therefore, acicular martensite formed after water quenching decreased, which reduced the thickness of the carburized layer.

INTRODUCTION

The massive accumulation of scrap is an urgent problem that needs to be solved. Increasing the amount of scrap used in the steelmaking process is the most direct method for solving this problem. Moreover, it is important for the increase of scrap ratio to promote the scrap melting.^{1,2}

Most previous studies have investigated the scrap melting mechanism through experiments and numerical calculations aimed toward increasing the metallic raw material scrap fraction.^{2–9} All the studies have indicated that scrap melting is a phase transformation phenomenon involving heat and mass transfer of carbon. In particular, the mass transfer of carbon has a significant effect on the melting process when the scrap carbon content is much lower than that of molten hot metal.³ Here, the melting rate is limited by mass transfer control, which decreases the scrap melting point to promote

scrap melting.^{4,5} Isobe⁶ proposed a heat and mass transfer model for scrap melting that considered the heat exchange between the hot metal and scrap. He pointed out that carbon diffusion from the hot metal to the scrap surface reduced its melting point. As a key parameter for describing the mass transfer process, the mass transfer coefficient has been discussed in many reports.^{2,9–16} The range of mass transfer coefficients under natural and forced convection was $10^{-6}\text{--}10^{-4} \text{ m/s}$ and $10^{-5}\text{--}10^{-4} \text{ m/s}$, respectively. However, there have been few analyses of the interfacial carbon diffusion phenomenon. Penz et al.¹⁷ explored this phenomenon at the scrap melting interface using EPMA. They pointed out that a steep carbon concentration gradient existed in the liquid, which started at an interface carbon concentration equal to the concentration on the solid side of the interface. Wei et al.¹⁸ investigated the melting characteristics of scrap in melts of varying carbon content and bottom-blowing gas flow rates. The microstructure of the scrap in the molten bath after different immersion times was observed using optical microscopy. Consistent with the results obtained by Penz et al., the microstructure

(Received July 29, 2021; accepted October 29, 2021;
published online November 23, 2021)

from the scrap surface to its interior was primary carbide \rightarrow acicular martensite \rightarrow original structure (dislocation martensite).

Other factors are known to affect interfacial carbon diffusion. Penz et al.¹⁷ indicated that there was a silicon-enriched layer during the carbon diffusion process. They inferred that the silicon-enriched layer was a retarding factor in the dissolution process. Liu et al.¹⁹ investigated the effect of silicon concentration on the melting behavior of scrap in hot metal. It was shown that the scrap melting rate decreased with an increase in the silicon content. Nevertheless, the interfacial carbon diffusion phenomenon and how it is affected by silicon have not been fully explained.

To improve the analysis of carbon diffusion at the solid–liquid interface during scrap melting, a novel laboratory investigation on interfacial carbon diffusion phenomenon was carried out. The microstructure of the scrap at the melting interface was observed using optical microscopy. The distribution and content changes of carbon and silicon were determined by EPMA. In addition, the effect of silicon concentration on carbon diffusion was explained from the perspective of the austenite phase area change in the Fe-Fe₃C phase diagram.

LABORATORY-SCALE EXPERIMENT AND THEORETICAL DESCRIPTION ON INTERFACIAL CARBON DIFFUSION

Experimental Set-Up

In a previous study, steel cylinders 100 mm in length and 10 mm in diameter were prepared from Q235 low-carbon steel and immersed in approximately 1 kg of molten pig iron with a carbon concentration of 4.61 wt.%.²⁰ The compositions of the experimental materials are listed in Table I. Samples immersed at bath temperatures of 1300°C, 1350°C, and 1400°C were selected for further analysis using EPMA.

The scrap cylinders were submerged for different times and then immediately quenched in water to avoid oxidation and prevent carbon diffusion. The samples were cut longitudinally using wire electrical discharge machining. Afterwards, the sectional surface of the samples was polished to 1 μm using SiC abrasive. An alumina suspension (1.0 μm) was used for the final polishing of samples before EPMA (SHIMADZU). The elements investigated were carbon and silicon. The size of the analyzed area was 402 \times 300 μm . After EPMA, the samples were

etched with nitric acid and optically examined using a metallograph (Leica DM4 M).

Theoretical Description of Carbon Diffusion

Scrap melting during the steelmaking process results from coupled heat and mass transfer. Carbon is the most important element in this process. As shown in Fig. 1a, the carbon mass transfer controls the melting process when the bath temperature is lower than the scrap melting point. The melting mechanism is that carbon diffuses from the hot metal into the surface of the scrap, which decreases its melting point. Subsequently, the scrap starts to melt once the melting point is lower than the bath temperature. According to previous studies and the results described herein, scrap melting can be divided into three stages:^{2,3,7–9} (1) The hot metal freezes on the surface of the scrap cylinder to generate a solidified layer until a maximum thickness is reached. (2) The solidified layer gradually melts until the original surface of the scrap cylinder is exposed. (3) The original scrap cylinder begins to melt, which is controlled by carbon mass transfer. Penz et al. summarized scrap melting into the following stages:¹⁷ stage 1: solidification and rapid remelting of a liquid hot metal layer on the surface of the cold scrap; stage 2: diffusive melting, depending on the carbon composition of the hot metal and scrap; stage 3: a forced or convective scrap melting stage when the temperature of the hot metal exceeds the melting temperature of the scrap. At this stage, only heat transfer should be considered, while heat and mass transfer work simultaneously in stage 1. In stage 2, the carbon content in the solid steel is much lower than that in the liquid melt, and only mass transfer must be considered. According to earlier work,²¹ scrap melting can be subdivided into four stages: formation of a solidified layer, rapid melting of the solidified layer, carburization, and carburization plus normal melting. This is consistent with other work.¹⁷ These numerous prior studies highlight the importance of carbon diffusion during scrap melting.

The Fe-Fe₃C phase diagram can be used to explain the mechanism of carbon diffusion.²⁰ Figure 1b shows this diagram (FactSage 7.0) where the contents of Mn and Si are set to 0.391 wt.% and 0.11 wt.%, respectively. The original conditions of the hot metal and scrap cylinder are (C_b , T_b) and (C_s , T_s), respectively. In the carbon diffusion stage, carbon is continuously transferred from the hot metal to the cylinder surface. The carbon concentration varies from the cylinder into the hot metal according to $C_s < C_s^* < C$. The scrap melting point varies along the liquidus line and decreases with increasing carbon content until it reaches T_L . According to previous studies, the melting point can be assumed to be the liquidus temperature obtained from a linear approximation of the Fe-C phase diagram.^{10–13,15,20} The blue points in Fig. 1 depict the specific isothermal

Table I. Composition of experimental materials (mass.%)

	C	Si	P	Mn	S
Steel cylinder	0.1675	0.11	0.041	0.391	0.124
Iron/carbon bath	4.61	0.42	0.17	0.33	0.04

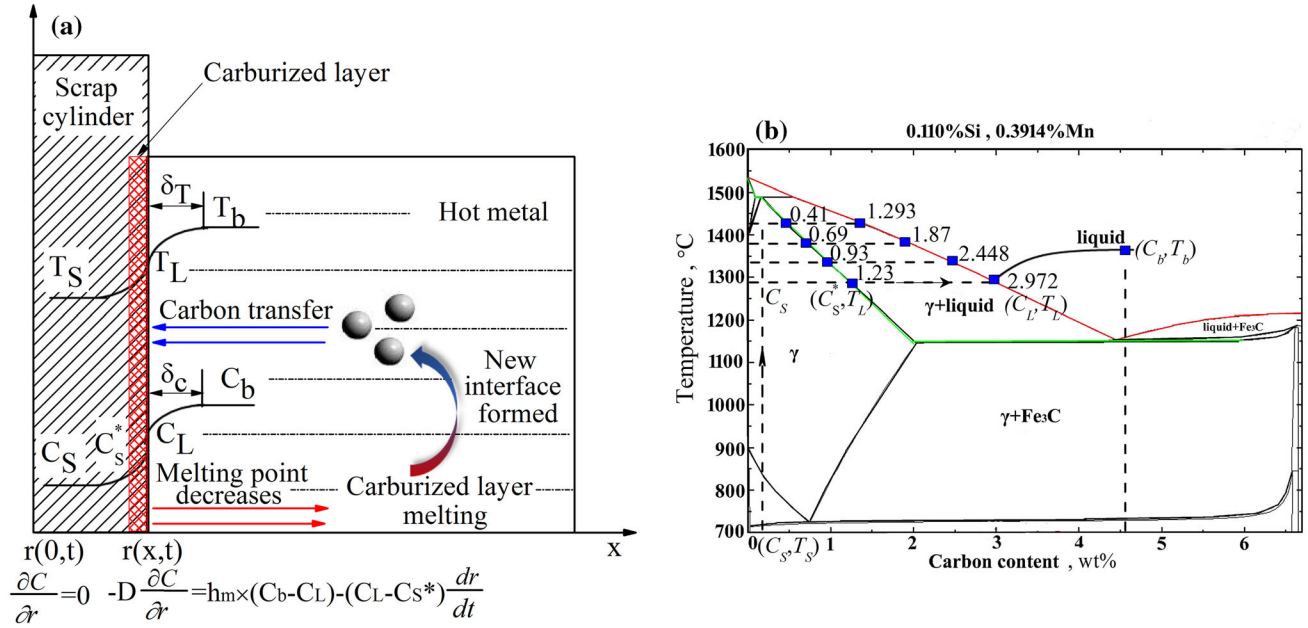


Fig. 1. Mechanism of scrap melting: (a) temperature/concentration profile and (b) Fe-Fe₃C phase diagram.

carbon concentrations of the scrap (C_s) and the assumed liquid hot metal composition C_b as well as the solidus (C_s^*) and liquidus (C_L) concentrations.

The carbon diffusion process from the scrap-hot metal interface into the solid scrap can be described by Fick's second law. If only the one-dimensional diffusion process in the radial direction is considered, the axisymmetric problem in the cylindrical coordinate system can be described by Eq. 1,⁴

$$\frac{\partial C}{\partial t} = D \left(\frac{\partial^2 C}{\partial r^2} + \frac{1}{r} \frac{\partial C}{\partial r} \right) \quad (1)$$

where c is the carbon content in wt.%. t is the time in s. D is the diffusion coefficient in m/s. r is the diffusion distance in m. At the beginning of melting,

$$C|_{t=0} = C_s \quad (2)$$

The carbon mass fraction in the solid scrap can be considered constant at large distance from the melting interface. The internal boundary conditions are expressed by Eq. 3.

$$\frac{\partial C}{\partial r} = 0 \quad (3)$$

The carbon mass balance at the scrap-hot metal interface is expressed by Eq. 4.

$$-D \frac{\partial C}{\partial r} = h_m \times (C_b - C_L) - (C_L - C_s^*) \frac{dr}{dt} \quad (4)$$

where h_m is the mass transfer coefficient.

RESULTS AND DISCUSSION

Microstructure and Carbon Distribution at the Solid–Liquid Interface

Carbon was diffused from the hot metal to the surface of the scrap in the stage of diffusive melting. The microstructure of the original cylinder prior to the experiment was ferrite and pearlite (supplementary Fig. S-1). The results at different immersion times of 1300–1450°C are depicted in Figs. 2, 3, 4. The microstructure and carbon distribution for the sample immersed at 1300°C for 60 s are used as examples to describe the carbon diffusion phenomenon at the interface. Figure 2a shows the microstructure obtained using optical microscopy. Figure 2b shows the EPMA surface scan results for the area corresponding to the red dashed box in Fig. 2a. Figure 2c shows the line scan result at the solid red line in Fig. 2a. As shown in Fig. 2a, the microstructure from the edge of the scrap to its interior is primary carbide → acicular martensite → original structure (dislocation martensite). The outermost layer is the solidified layer after cooling, which was not in close contact with the surface of the scrap. There is an obvious interface between the outermost solidified layer and the scrap surface. It appears as a bright area in the scrap material. Acicular martensite formed with a decrease in the carbon content. A small amount of retained austenite can also be observed. The acicular martensite transformed into dislocation martensite, which was formed due to water quenching. Previous studies have also reported that carbon diffusion occurs at the scrap-hot-metal interface.^{17,18} It was shown that the microstructure from the edge of the scrap to its

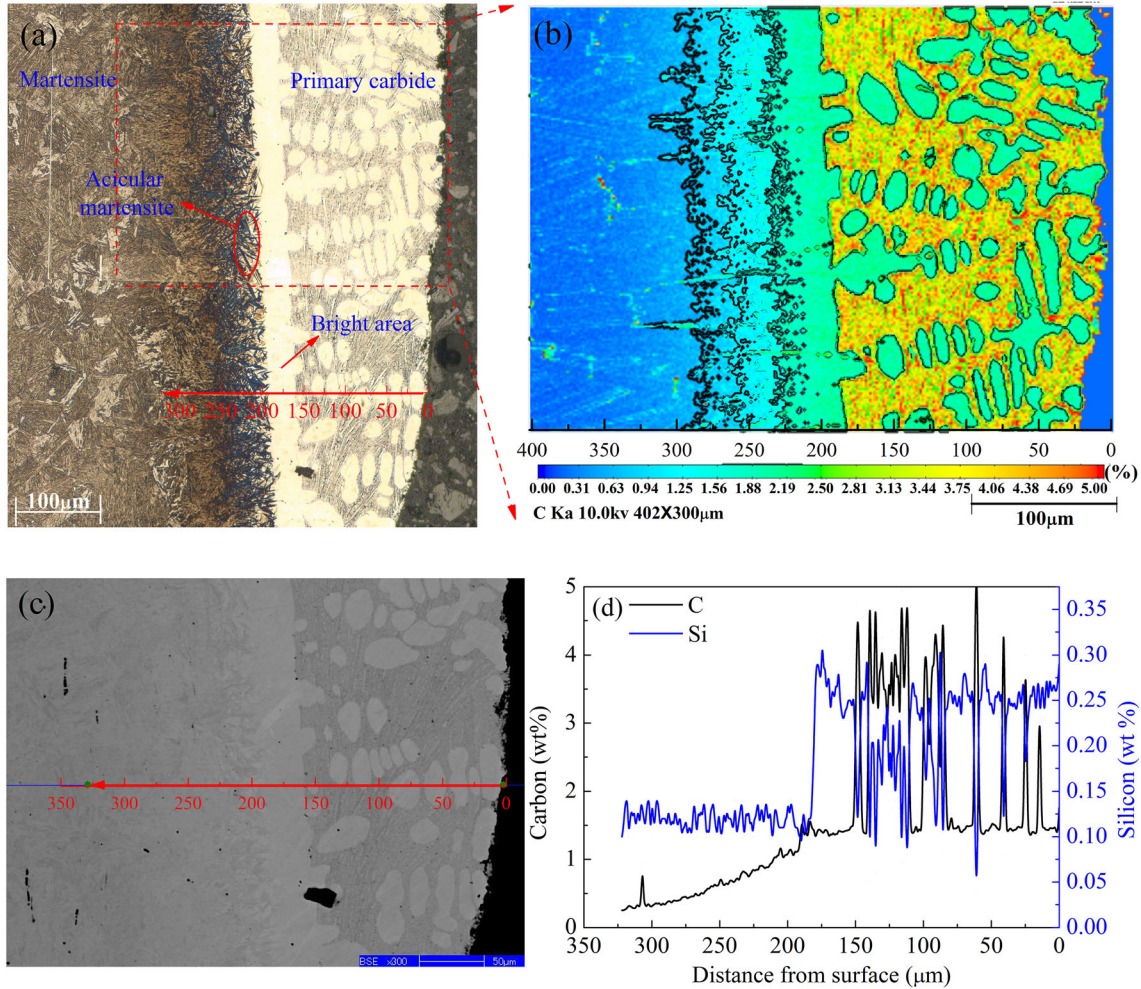


Fig. 2. Microstructure and EPMA results at 1300°C for 60 s: (a) microstructure of sample, (b) surface scan of carbon obtained by EPMA, (c) line scan position, and (d) line scan of carbon and silicon obtained by EPMA.

interior was primary carbide → bright area → matrix structure of scrap.

As shown in Fig. 2b, c, and d, there is a carbon concentration gradient from the edge of the scrap to its interior. The carbon content gradually decreases, which is consistent with the change in the microstructure. The microstructure of the outermost layer is primary carbide, whose carbon content exceeds 4 wt.%. Moving inward, the carbon content rapidly decreases to 1–1.5 wt.%, which is consistent with that of acicular martensite. The results confirm the existence of an acicular martensite layer. Meanwhile, an approximately 40 μm silicon-enriched layer appears in which the silicon content (0.25–0.3 wt.%) is more than twice that of the substrate (0.11 wt.%). Finally, the carbon content gradually decreases to 0.2 wt.% and then remains unchanged. The microstructure is dislocation martensite. Therefore, the change in the carbon content is consistent with that of the microstructure.

Effect of Bath Temperature on Interfacial Carbon Diffusion

Increasing the temperature is beneficial for the diffusion process. The following two important definitions can be made.¹⁷ (1) The position where the carbon content gradually decreased to close to the initial carbon content (0.17% wt.%) of the scrap was defined as the end of carbon diffusion. (2) To eliminate the influence of the outermost solidified layer on the carbon diffusion depth, the position where the solidified layer contacted the bright area was defined as the starting point for calculating the carbon diffusion depth. In Fig. 5a, the convective heat transfer from the hot metal to the surface of the scrap and the heat conduction inside the scrap mainly occurred in the formation stage of the solidified layer (5 s). The carbon diffusion depth is small (approximately 100 μm). At 10 s, the parent scrap was exposed and started to melt with carbon diffusion. The carbon diffusion depth is approximately 200 μm. Penz et al.¹⁷ found that the carbon diffusion depths at different immersion times were

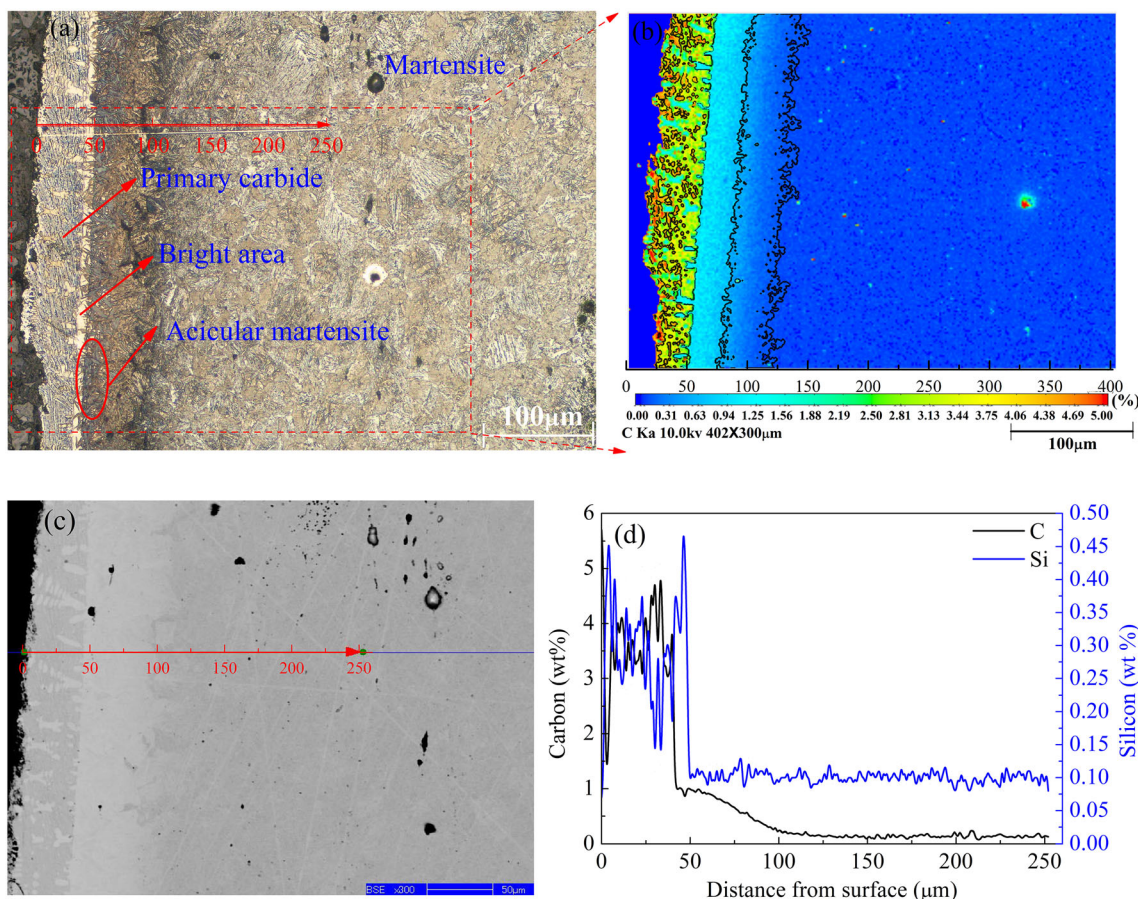


Fig. 3. Microstructure and EPMA results at 1350°C for 5 s: (a) microstructure of sample, (b) surface scan of carbon obtained by EPMA, (c) line scan position, and (d) line scan of carbon and silicon obtained by EPMA.

almost equal. The carbon diffusion depth at 1350°C is approximately 200 μm. The results in Fig. 5 are consistent with those obtained by Penz et al. Therefore, the carbon diffusion at the solid–liquid interface during scrap melting is mainly affected by the bath temperature. The carbon diffusion depth was less affected by immersion time. In Fig. 5b and c, the profile at the formation stage of the solidified layer (1350°C for 5 s and 1400°C for 2 s) is not well developed. The carbon diffusion depths at 1300°C and 1350°C are 200 μm and 220 μm, respectively. The depth reached approximately 160 μm within 5 s when the bath temperature was 1400°C. At 60 s, the position where the carbon was 0.17 wt.% was not measured because the measurement position was close to the sample surface. However, the diffusion depth exceeded 200 μm according to the development trend of the profile. In summary, the carbon diffusion depth increased with increasing bath temperature.

This phenomenon can be explained by the well-known equation $D = D_0 e^{-\frac{Q}{RT}}$, where D_0 is the diffusion constant, Q is the diffusion activation energy in J/mol, R is the gas constant in J/(kg·K), and T is the thermodynamic temperature in K. The vibration energy of the carbon atoms is greater at higher bath

temperatures; the probability of atoms migrating across the potential energy barrier owing to energy fluctuations increases; consequently, the diffusion coefficient increases. Therefore, carbon diffusion is promoted at higher bath temperatures.²² In addition, the experimental results of scrap melting also showed that the melting time at higher bath temperatures was shorter.

Effect of Silicon on Interfacial Carbon Diffusion

The results obtained from EPMA and optical microscopy in Figs. 2–4 show a bright area between the outer solidified layer and the scrap interface. The comparison between the EPMA surface and line scan results in Figs. 2–4 shows that the silicon content in the bright area is much higher than that of the substrate. Conversely, the carbon content is stable at approximately 1 wt.% and gradually decreases. In other words, a phenomenon of high silicon and low carbon appeared in this area. In Fig. 6, the enrichment of silicon during carbon diffusion is illustrated using the sample held at 1300°C for 60 s as an example. The silicon-enriched layer is approximately 40 μm thick, and the silicon content is approximately 0.25% wt.%, which is more

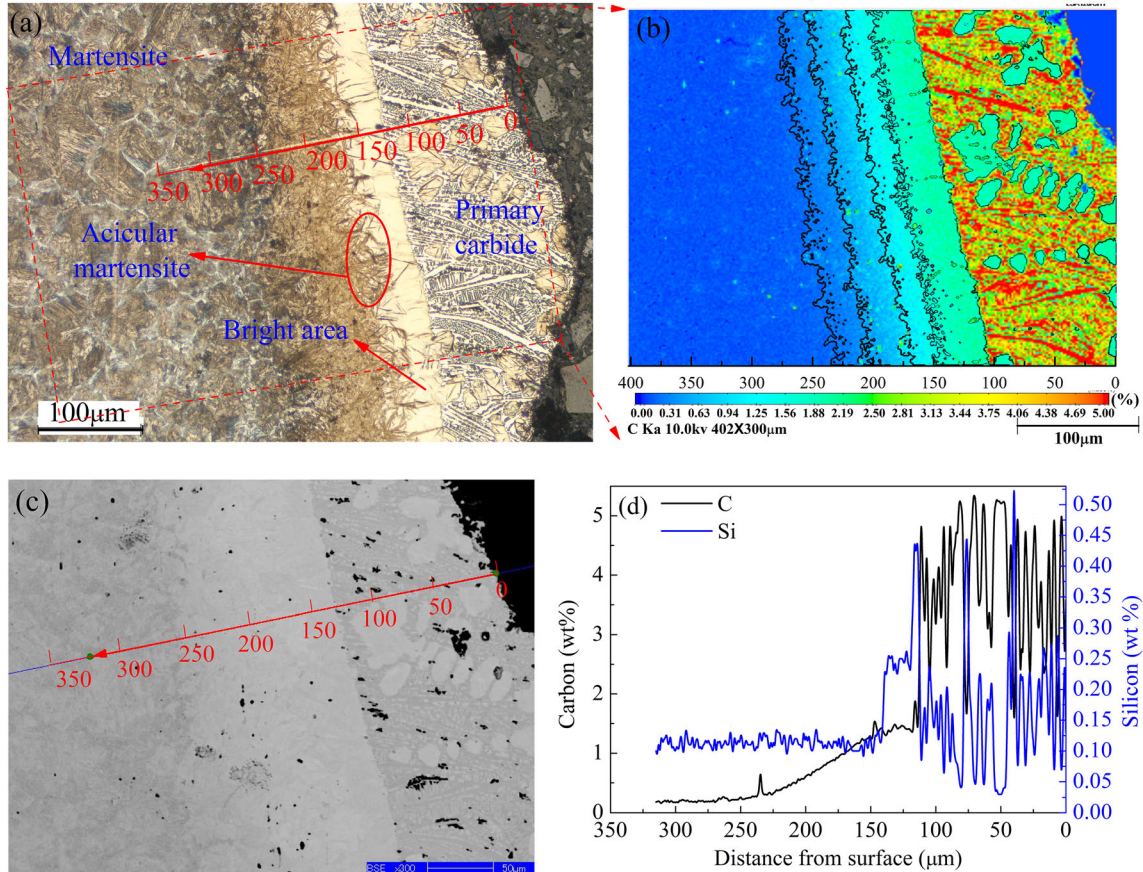


Fig. 4. Microstructure and EPMA results at 1400°C for 5 s: (a) microstructure of sample, (b) surface scan of carbon obtained by EPMA, (c) line scan position, and (d) line scan of carbon and silicon obtained by EPMA.

than twice that of the substrate (0.11 wt.%). The carbon content gradually decreases from 1.49 wt.% at the interface. The same phenomenon was observed at the other bath temperatures.

Penz et al.¹⁷ also found an enrichment of silicon. They illustrated that the dispersed silicon oxides in the parent scrap would remain at the location of the lowest energy, which was at the interface. The dispersed silicon oxides can be reduced by the transferred carbon, which may be a retarding factor in the dissolution process. In addition, Wang²³ reported that silicon is a non-carbide-forming element that can increase carbon activity. However, the mobility of the iron atoms was significantly reduced in the austenite due to silicon. As a result, the binding energy of iron in the solid solution increased, and the carbon diffusion was hindered. The effect of silicon on the austenite phase region in the Fe-Fe₃C phase diagram can be used to illustrate this phenomenon. Figure 7a and b shows these phase diagrams for 0.391% Mn and (0.391% Mn + 0.11% Si), respectively. Compared with the temperature changes at different points, it is shown that the A₃ temperature increases from 893.4°C to 900.7°C when 0.11 wt.% Si is added. The A₄ temperature decreases from 1403.1°C to 1398.9°C, while the eutectic point (E) and the eutectoid point

(S) move towards the left. The eutectoid temperature increases from 723.39 to 725.27°C. These changes lead to a reduction in the area of the austenite phase region. In Fig. 7c, the austenite phase region decreases with an increase in the silicon content. Wang²³ also pointed out that the addition of Si causes the austenite phase region to shrink while expanding the α phase region. The austenite phase region disappeared when the silicon content was sufficiently high.

In this work, the scrap that had been immersed in hot metal for different times and quenched showed microstructural changes from the surface to the interior of primary carbide → acicular martensite → dislocation martensite. The austenite transformed into acicular martensite at a higher temperature by rapid cooling. Previous studies¹⁷ reported that the temperature of scrap during melting reaches the austenite temperature. Subsequently, acicular martensite was formed after quenching in water. For the scrap with 0.11 wt.% silicon, the amount of acicular martensite formed after water quenching decreased because of the reduction in the size of the austenite phase region. This was manifested as a decrease in carbon diffusion depth.

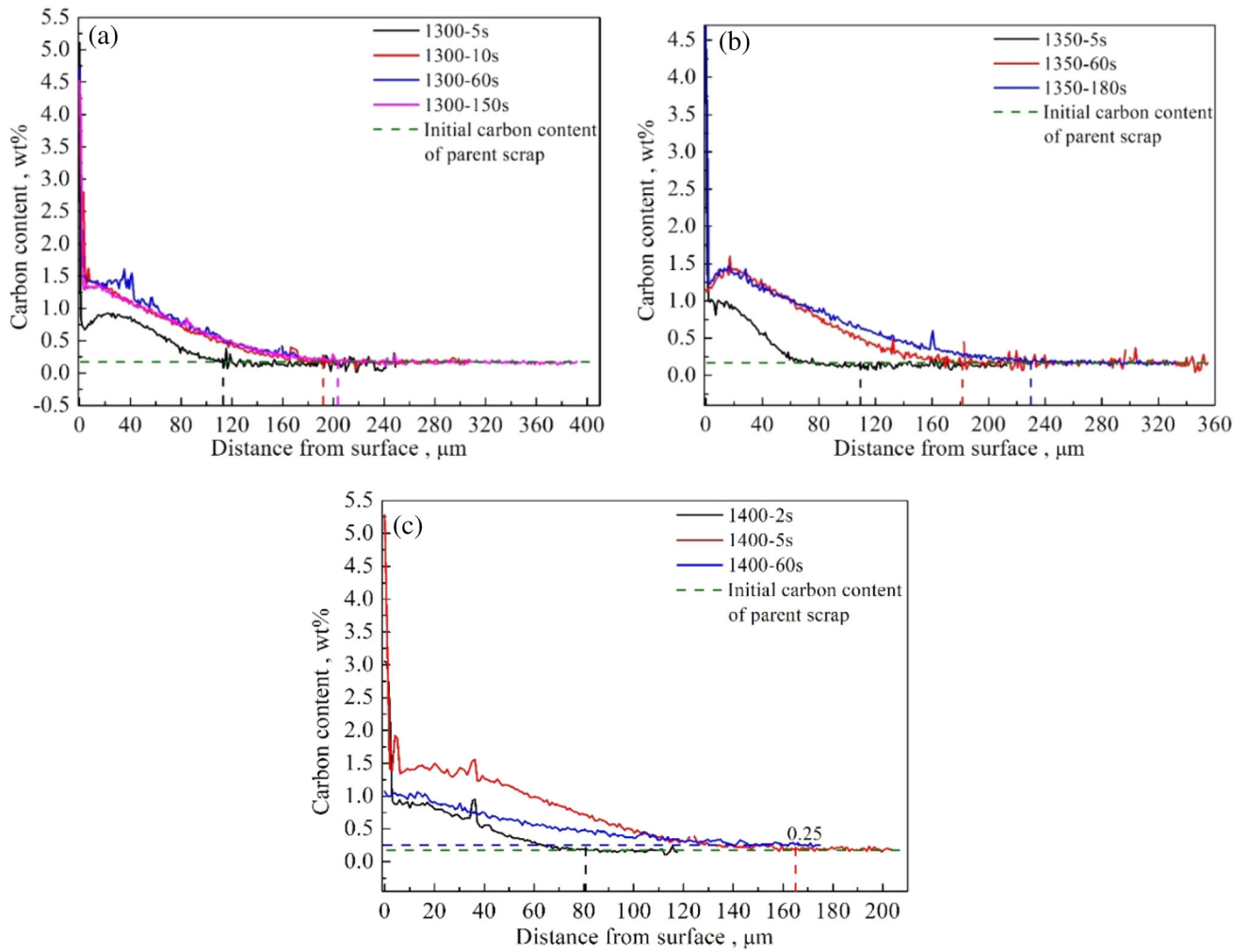


Fig. 5. Interfacial carbon distribution at (a) 1300°C, (b) 1350°C, and (c) 1400°C.

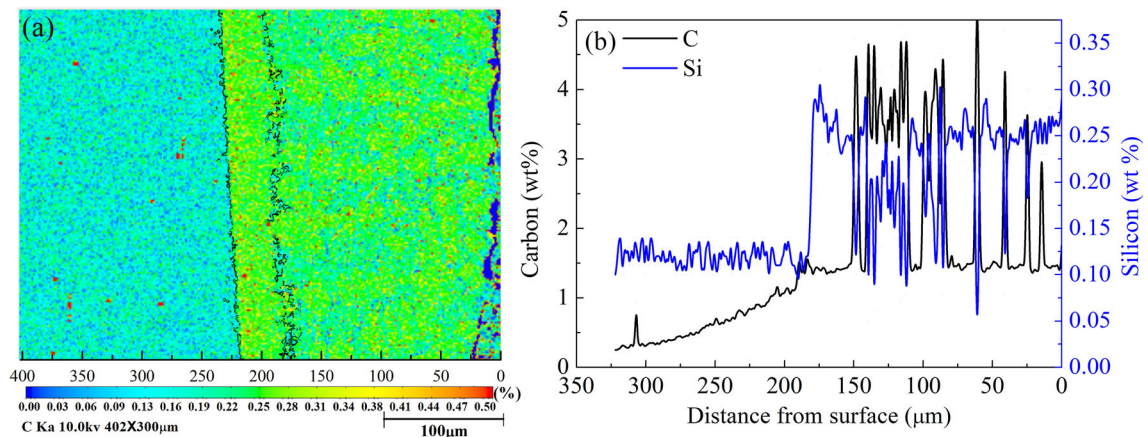


Fig. 6. Silicon distribution and EPMA results at 1300°C for 60 s: (a) surface scan of silicon and (b) line scan of carbon and silicon obtained by EPMA.

CONCLUSION

A laboratory investigation on interfacial carbon diffusion phenomenon was carried out to obtain the scrap microstructural changes at the melting

interface, element distribution, and elemental content using optical microscopy and EPMA. Meanwhile, the phenomenon of carbon diffusion at the solid-liquid interface during scrap melting and the

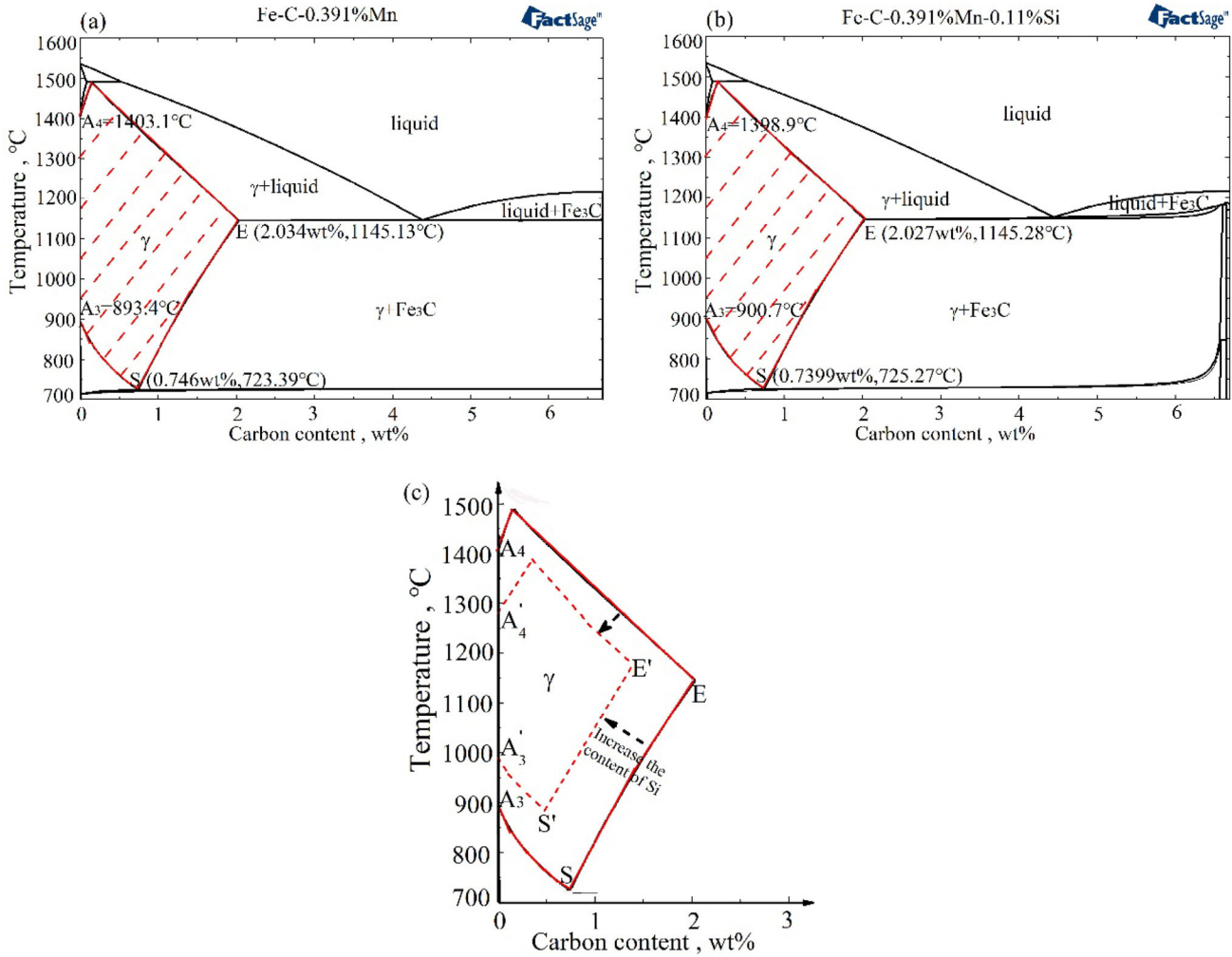


Fig. 7. Fe-Fe₃C phase diagram with (a) 0.391% Mn, (b) 0.391% Mn and 0.11% Si, and (c) the influence of silicon on the austenite phase region.

effect of silicon concentration on carbon diffusion were illustrated. The main conclusions are as follows.

- (1) The microstructural path from the scrap surface to its interior was primary carbide → acicular martensite → original structure (dislocation martensite). The carbon content in the outermost layer (primary carbide) exceeded 4 wt.%, rapidly reduced to 1–1.5 wt.%, gradually decreased to 0.2 wt.%, and then remained unchanged. The carbon content changes were consistent with the observed microstructures.
- (2) The depth of the carbon diffusion layer increased with increasing bath temperature. These depths were 200 μm and 220 μm at 1300°C and 1350°C, respectively. The depth reached approximately 160 μm within 5 s when the bath temperature was at 1400°C.
- (3) A silicon-enriched layer appeared in which the silicon content (0.25–0.3 wt.%) was more than

twice that of the substrate (0.11% wt.%). This may be a retarding factor for carbon diffusion. The changes in the Fe-Fe₃C phase diagram when silicon is considered showed that the size of the austenite phase region should decrease with increasing silicon. Therefore, the amount of acicular martensite formed after water quenching decreased, which reduced the carbon diffusion depth.

ACKNOWLEDGEMENTS

This work was supported by the National Key R&D Program of China (no. 2019YFC1905701) and the Key Projects of NSFC (U1960201).

CONFLICT OF INTEREST

The authors declare that they have no conflict of interest.

SUPPLEMENTARY INFORMATION

The online version contains supplementary material available at <https://doi.org/10.1007/s11837-021-05022-0>.

REFERENCES

1. F. Oeters and R.M. Ni, in *Metallurgy of Steelmaking* (Metallurgical Industry Press, Beijing, 1997), pp. 479–481.
2. F.M. Penz, and J. Schenk, *Steel Res. Int.* 90, 1. (2019).
3. H. Gaye, M. Wanin, P. Gugliermana, and P. Schittly, in *Proceeding of 68th Steelmaking Conference, Detroit, USA* (1985).
4. J.H. Li, *Kinetics of steel scrap melting in liquid steel bath in an electric arc furnace* (McMaster University, 2007).
5. J. Szekely, Y.K. Chuang, and J.W. Hlinka, *Metall. Mater. Trans. B* 3, 2825. (1972).
6. K. Isobe, H. Maede, K. Ozawa, K. Umezawa, and C. Saito, *Tetsu-to-Hagane* 76, 2033. (1990).
7. R.D. Pehlke, P.D. Goodell, and R.W. Dunla, *Trans. Metall. Soc. AIME* 233, 1420. (1964).
8. H. Sun, Y. Liu, and C. Lin, *International Congress on the Science & Technology of Steelmaking* (Beijing International Convention Center, Beijing, 2015), pp 136–139.
9. A.K. Shukla, B. Deo, and D.G.C. Robertson, *Metall. Mater. Trans. B* 44, 1407. (2013).
10. J.K. Wright, *Metall. Mater. Trans. B* 20, 363. (1989).
11. W.Y. Yang, *Iron Steel* 52, 27. (2017).
12. W.Y. Yang, X.G. Zhang, and Y. Yang, *Iron Steel Scrap China* 22, 1. (2012).
13. Y.U. Kim, and R. Pehlke, *Metall. Mater. Trans. A* 5, 2527. (1974).
14. M. Kosaka, and S. Minowa, *Tetsu-to-Hagane* 53, 983. (1967).
15. K. Mineo, and M. Susumu, *Tetsu-to-Hagane* 52, 537. (1966).
16. K. Mineo, and M. Susumu, *Tetsu-to-Hagane* 53, 1467. (2010).
17. F. Penz, J. Schenk, and R. Ammer, *Materials* 12, 1. (2019).
18. G. Wei, R. Zhu, T. Tang, and K. Dong, *Ironmak. Steelmak.* 46, 609. (2019).
19. C. Liu, H. Zhang, Q. Fang, X. Liu, and H. Ni, *Metall. Mater. Trans. B* 51, 1668. (2020).
20. M. Gao, S.F. Yang, and Y.L. Zhang, *Ironmak. Steelmak.* 47, 1006. (2020).
21. M. Gao, J.T. Gao, Y.L. Zhang, and S.F. Yang, *Int. J. Miner. Metall. Mater.* 28, 380. (2021).
22. Z. Cui and Y. Tan, *Metal Science and Heat Treatment* (Harbin Institute of Technology Press, 2004), pp. 225–228.
23. X. Wang, *Metallic Materials* (China Machine Press, Beijing, 1989), pp. 23–25.

Publisher's Note Springer Nature remains neutral with regard to jurisdictional claims in published maps and institutional affiliations.